Author Manuscript

Author Manuscript

Author Manuscript

Author Manuscript

HHS Public Access

Author manuscript

Nat Biotechnol. Author manuscript; available in PMC 2016 June 01.

Published in final edited form as:

Nat Biotechnol. 2015 December ; 33(12): 1280–1286. doi:10.1038/nbt.3415.

Soft, stretchable, fully implantable miniaturized optoelectronic systems for wireless optogenetics

Sung Il Park[1,2,*], **Daniel S. Brenner**[3,*], **Gunchul Shin**[1,2,*], **Clinton D. Morgan**[3,*], **Bryan A. Copits**[3], **Ha Uk Chung**[1,2], **Melanie Y. Pullen**[3], **Kyung Nim Noh**[1,2], **Steve Davidson**[3], **Soong Ju Oh**[1,4], **Jangyeol Yoon**[1,2,5], **Kyung-In Jang**[1,2], **Vijay K. Samineni**[3], **Megan Norman**[3], **Jose G. Grajales-Reyes**[3], **Sherri K Vogt**[3], **Saranya S. Sundaram**[3], **Kellie M. Wilson**[3], **Jeong Sook Ha**[5], **Renxiao Xu**[6], **Taisong Pan**[6], **Tae-il Kim**[5], **Yonggang Huang**[6], **Michael C. Montana**[3], **Judith P. Golden**[3], **Michael R. Bruchas**[3], **Robert W. Gereau IV**[3], and **John A. Rogers**[1,2]

[1]Department of Materials Science and Engineering, University of Illinois at Urbana-Champaign, Urbana, IL, USA

[2]Frederick Seitz Materials Research Laboratory, University of Illinois at Urbana-Champaign, Urbana, IL, USA

[3]Washington University Pain Center and Department of Anesthesiology, Washington University School of Medicine, St. Louis, Missouri, USA

[4]Department of Materials Science and Engineering, Korea University, Seoul, Republic of Korea

[5]Department of Chemical and Biological Engineering, Korea University, Seoul, Republic of Korea

[6]Department of Mechanical Engineering, Northwestern University, Chicago, IL, USA

Abstract

Users may view, print, copy, and download text and data-mine the content in such documents, for the purposes of academic research, subject always to the full Conditions of use:http://www.nature.com/authors/editorial_policies/license.html#terms

To whom correspondence should be addressed: ; Email: jrogers@illinois.edu and ; Email: gereaur@wustl.edu

*These authors contributed equally to this work

Author Contributions

S.I.P. designed wireless optoelectronic systems, fabricated devices, tested devices, made wireless measurements, conducted simulations of wireless performance, designed experiments, generated figures, wrote and edited the manuscript. D.S.B. designed sciatic nerve devices, implanted devices, tested mice in behavior, designed experiments, performed immunostaining, generated figures, wrote and edited the manuscript. G.S. designed and fabricated spinal cord devices, tested devices, generated figures, wrote and edited the manuscript. C.D.M. designed spinal cord devices, implanted devices, tested mice in behavior, designed experiments, performed immunostaining, generated figures, wrote and edited the manuscript. B.A.C. performed immunostaining and quantification, electrophysiology experiments, generated figures. H.U.K. & K.N.N. fabricated devices and tested devices. S.D. performed experiments, implanted devices, generated figures. S.J.O., J.Y., and K.I.J. made contributions to fabrication and testing of devices. V.K.S. performed experiments, immunostaining, generated figures. M.N. performed immunostaining and quantification of slides, as well as mouse breeding. J.G.G.R. performed experiments, generated figures. S.K.V. performed immunostaining and mouse breeding. S.S. performed immunostaining and mouse breeding. K.M.W. performed immunostaining. J.S.H. made contributions to fabrication and testing of devices. R.X., T.P., & Y.H. performed mechanical simulations of device tolerance levels.
M.C.M. designed experiments and generated figures. J.P.G. performed immunostaining, generated figures, performed behavioral experiments, and edited the manuscript. M.R.B. designed experiments. R.W.G. & J.A.R. oversaw all experiments and data analysis, designed experiments and devices, wrote and edited the manuscript.

Competing Financial Interests Statement

The authors declare no competing interests as defined by Nature Publishing Group, or other interests that might be perceived to influence the results and discussion reported in this paper.

Author Manuscript Author Manuscript Author Manuscript Author Manuscript

Optogenetics allows rapid, temporally specific control of neuronal activity via targeted expression and activation of light-sensitive proteins. Implementation typically requires remote light sources and fiber-optic delivery schemes that impose significant physical constraints on natural behaviors. In this report we bypass these limitations using novel technologies that combine thin, mechanically soft neural interfaces with fully implantable, stretchable wireless radio power and control systems. The resulting devices achieve optogenetic modulation of the spinal cord and peripheral nervous system. This is demonstrated with two form factors; stretchable film appliques that interface directly with peripheral nerves, and flexible filaments that insert into the narrow confines of the spinal epidural space. These soft, thin devices are minimally invasive, and histological tests suggest they can be used in chronic studies. We demonstrate the power of this technology by modulating peripheral and spinal pain circuitry, providing evidence for the potential widespread use of these devices in research and future clinical applications of optogenetics outside the brain.

The use of optogenetics in the brain has revolutionized the interrogation of neural circuitry by enabling temporal and spatial control of neuronal function. However, attempts to apply optogenetic studies to tissues beyond the brain have been stymied by the inability to target peripheral and spinal circuits in freely-moving animals. Studies to date have primarily utilized cumbersome tethered fiber optic cables or light emitting diode (LED) arrays to activate opsins that are expressed transgenically or delivered through gene therapy.[1–3] Although these experimental approaches have utility, physical tethers impede movement, which can alter behavior and the natural motion of animals in complex environments. Additionally, the fixation of fiber-optic cables requires physical bonding to a static skeletal feature such as the skull, and external fixtures can cause device loss due to damage by the animal, a cage mate, or by inadvertent damage from housing or during experiments. These fibers can also damage the surrounding neural tissue during insertion or during fiber coupling due to relative motion of the hard fiber against soft tissues.[4, 5]

Thin, injectable polymer filaments with integrated, cellular-scale LEDs and externally mounted wireless power harvesting systems[6–9] represent attractive alternatives, but cannot illuminate spatially challenging and highly mobile areas like peripheral nerves or the spinal cord, which are critical to the study of the extracranial circuits involved in sensory input and motor output. Recently developed fully implantable devices with radio frequency powered LEDs achieve some capabilities in these contexts[10], however these devices utilize hard materials and geometrically thick designs which limits their potential for chronic biocompatibility and integration with soft tissues of the nervous system.

Miniaturized, biocompatible devices that can safely interface with peripheral neural tissue and illuminate challenging areas are needed to advance the technology support for advanced optogenetic studies not only of the brain, but also of issues related to chronic pain, itch, and other neurological disorders. The development of suitable devices requires managing heat generation and power delivery, enabling robust remote activation with uniform, natural operation across cage configurations and animal species, achieving power delivery over large areas, and realizing miniaturization with thin geometries and low-modulus, elastic mechanics for chronic tissue compatibility.[8]

Author Manuscript Author Manuscript Author Manuscript Author Manuscript

Here we present miniaturized, soft wireless optoelectronic systems with versatile layout options that are fully compatible with advanced methods for mass production in semiconductor device manufacturing and capable of complete, minimally invasive implantation over multiple neural interfaces. The low modulus mechanics of these biocompatible devices allows their implantation as thin appliques and/or soft injectable filaments, without the need for skeletal fixation, thereby permitting experiments in regions that would be otherwise impossible. We demonstrate that these devices can specifically and reversibly activate both peripheral and spinal pain circuits in freely behaving, untethered mice. Detailed chronic studies and histological evaluations show the essential benefits of soft, compliant and fully implantable device technologies of this type.

The miniaturized wireless optoelectronic systems are composed of a radio frequency harvesting unit that receives signals from a transmitter, rectifies them, multiplies the voltages, and routes the resulting direct-current output to the LEDs (a turn-on voltage of 2.7 V, 470 nm wavelength). The antenna and LEDs are connected with serpentine Ti/Au electrical interconnects, and the circuit is encapsulated by polyimide (40 μm width, 3 μm thickness) and a low modulus silicone elastomer (~0.5 MPa, 100 μm thickness). This process yields soft, system-level mechanics (effective modulus of ~1.7 MPa) capable of accommodating anatomical shapes and natural motions.[6–9] A schematic view of a completed system appears in Fig. 1a. Supplementary Note 1 and Supplementary Fig. 1–3 provide details of the components and the circuit layouts, as well as the electrical and mechanical characteristics. Fabrication steps and equipment are detailed in Supplementary Table 1 and **Online Methods**.

The mechanical compliance, miniaturized geometry (0.7 mm × 3.8 mm × 6 mm), and lightweight construction (16 mg) of these devices enables implantation into anatomical regions that were previously inaccessible due to physical constraints. In comparison with previous technology, these devices are significantly thinner, softer, and more flexible (Supplementary Note 1).[8,10, 11] Here, we illustrate the deployment of these devices underneath muscle for optogenetic stimulation of a peripheral nerve (Fig. 1b), and in the epidural space for optogenetic control in the spinal cord (Fig. 1c). Peripheral nerve illumination is achieved with a soft applique that is implanted with the antenna in a subcutaneous pocket with an LED extension that traverses under the gluteus maximus to the sciatic nerve. The distal extension with the LEDs includes wings (1 mm × 3 mm) that anchor the LED tip in the gluteal pocket once the muscular architecture has been repaired with suture (Fig. 1b, d, f). Spinal illumination is achieved by implantation under the vertebra in the epidural space, which is accessed by laminectomy of the T13 spinous process (Fig. 1c, e, g). This placement centers the narrow part of the device (380 μm × 8 mm) over the lumbar spinal cord.

The key to miniaturizing these devices is a stretchable antenna that harvests RF power through capacitive coupling between adjacent serpentine traces (Supplementary Fig. 4), thereby lowering the resonant frequency and therefore the dimensions of the antenna.[12] For operation at 2.34 GHz, this design requires an area of only 3 × 3 mm, a 100-fold reduction in volume and weight compared to conventional rigid antennas.[8] This antenna also features a wide bandwidth, which is essential for reliable activation of the devices since the center

Author Manuscript Author Manuscript Author Manuscript Author Manuscript

frequency of the receiving antenna must be similar to that of the transmitting antenna to efficiently harvest transmitted power. The center frequency describes the frequency range where an antenna absorbs energy most effectively and corresponds to the range of frequencies that minimize the scattering parameter (S_{11}). A lower S_{11} indicates that less incident energy is reflected off the antenna and therefore more of that energy is absorbed. The wide bandwidth (200 MHz) of the stretchable antenna allows it to harvest RF power from a much wider range of transmitting frequencies than conventional patch antennae (bandwidth of 50 MHz) (Supplementary Fig. 4d). This characteristic reduces the likelihood that a mismatch between the receiver and transmitter will prevent device activation. The S_{11} and center frequency in these devices are also affected by the physiological environment, which is detailed in Supplementary Note 2 and Supplementary Fig. 5.

The capacitive coupling that powers these devices can be diminished if strain deforms the metallized traces and increases the sizes of the gaps between them. To assess the reliability of these antennae under biological strain, we modeled and tested performance under worst-case scenarios (30 % strain) (Fig. 2a–b, Supplementary Fig. 5). Simulations show that while uniaxial strains of ~10 % increase the gap size in the direction of the strain, they reduce the gap size in the orthogonal direction by up to 50 % (Supplementary Fig. 6). As a result, the decrease in coupling due to increased gap size is balanced by enhanced coupling in the orthogonal direction, such that the harvesting efficiency of the antenna is largely unaffected (Fig. 2a–b).

While strain does not alter the efficiency of capacitive coupling, it does shift the center frequency of the antenna toward lower frequencies (Fig. 2a–b). However, the magnitudes of the strain-induced shifts in the center frequency are small compared to the large bandwidth (Supplementary Fig. 4d), such that the net result of supraphysiological strain application is a 12 % decrease in coupling efficiency due to center frequency shifts (Fig. 2a, b middle). This translates to a modeled optical power output decrease of only a few percent, suggesting that physiological strain is unlikely to significantly impair device function (Fig. 2a, b right). This modeling is confirmed by examples of devices functioning reliably under deformation significantly exceeding that expected in animals (Supplementary Fig. 7). Additionally, images and a movie of a mouse with a device interfaced to the sciatic nerve while running (Supplementary Fig. 8, Supplementary Movie 1) and a picture of successful wireless operation 6 months after implantation (Fig. 1f) support that these devices function reliably under physiological strain.

In addition to physical strain, other concerns for long-term implantation of electrical devices in animals include heat generation and long-term durability. Infrared imaging of an anesthetized mouse during device operation reveals that an optical power density of 10 mW/mm^2 (40 % duty cycle; 20 Hz period; 20 ms pulse width) does not cause detectable temperature changes (Fig. 2c). Experimental studies using implantable thermal sensors show similar trends (Supplementary Fig. 9, Supplementary Note 3). Studies also show that exposure to biological conditions does not significantly alter device operation or durability; devices retain full functionality for 2 months when immersed in 37 °C saline, and for 6 days in saline at supraphysiological temperatures (90 °C) (Fig. 2d). In terms of mechanical stability, these devices can be cycled $>10^5$ times without a detectable loss in optical power

Author Manuscript Author Manuscript Author Manuscript Author Manuscript

(Fig. 2e). The robustness suggested in these *in vitro* assays is reinforced by the fact that 76 % (31/41) of devices that were implanted for use in this work were still functional after 1 week in the animals. Two sciatic nerve devices retained reliable activation at least every month for 6 months after implantation, and of five sciatic nerve devices where reimplantation in new host mice after initial removal was attempted, three remained functional for 3 weeks after reimplantation. All of these observations suggest that heat generation, hydration effects, and durability are not obstacles for the use of these devices in animals.

For the devices to be useful in behavior experiments, the RF transmission (TX) systems must enable continuous operation throughout a location of interest (e.g., the homecage or testing arena), at field strengths that lie below IEEE and FCC guidelines. A configuration of four TX antennas connected to a common RF power supply (Fig. 2f) provides total average RF power that is sufficient for operation (~2 W) throughout the volume of the cage, and is capable of activating multiple devices in the same region (Fig. 2g). These devices can be activated reliably up to 20 cm from the transmitters, which is 10 times the reported range of any previous systems[8, 11] (Supplementary Fig. 10). Under these conditions, calculated distributions of the specific absorption rate (SAR; a measure of the rate at which RF energy is absorbed by the body) reveal that the SAR falls well below safety guidelines.[13] This configuration allows consistent device activation even with rapid changes in receiver location and orientation (Fig. 2h–j). This is demonstrated using long-exposure images captured during motion of an operating device; continuous streaks of light illustrate activation of the devices regardless of device position or orientation (Fig. 2i–j). Further discussion of the transmission efficiency with moving animals can be found in Supplementary Notes 4–5 and Supplementary Fig. 10–12.

To determine the utility of these optoelectronic devices in studies of pain pathways, we test whether they can modulate pain-related behaviors of mice expressing ChR2 in all sensory neurons or in subpopulations of sensory neurons responsible for detection of noxious stimuli (nociceptors). Mice expressing ChR2 in all sensory neurons were generated using a cre recombinase-based transgenic approach where cre recombinase expression is driven by the promoter of the sensory neuron-specific gene Advillin (Advillin-ChR2; Fig. 3a).[14, 15] Electrophysiological studies show that Advillin-ChR2 sensory neurons can be consistently activated by blue light (Fig. 3b–c, Supplementary Note 7), and immunohistochemical studies demonstrate that ChR2 is present in mid-axon, in the DRG, and in the central terminals of sensory neurons (Fig. 3d–f, Supplementary Note 8). Similar results are observed in mouse lines where ChR2 expression is restricted to nociceptor populations (TrpV1-ChR2, SNS-ChR2; see Supplementary Notes 6–8, Supplementary Fig. 13–17). Detailed electrophysiological characteristics of TrpV1-ChR2 dorsal root ganglion neurons can be found in Supplementary Table 2.

Previous studies have shown that illumination of peripheral nerve terminals using an external light source on the skin induces spontaneous pain behaviors and place aversion in mice expressing ChR2 in sensory neurons.[1, 3] For these implantable devices to be viable for *in vivo* pain studies, illumination of ChR2-expressing axons (shown schematically in Fig. 4a) must generate action potentials. Consistent with this hypothesis, fiber-optic laser

Author Manuscript Author Manuscript Author Manuscript Author Manuscript

illumination of the exposed sciatic nerve in TrpV1-ChR2 mice produces reflexive withdrawal behaviors (Supplementary Fig. 18). It is also critical that device implantation not induce nerve injury or impair function. Devices implanted over the sciatic nerve for two weeks produce no signs of injury and no infiltration of immune cells compared to the contralateral nerve (Supplementary Fig. 19–20), and produce no motor impairment, even when running (Supplementary Movie 1). This is quantified using the accelerating rotarod and open field tests (OFT), indicating that the devices do not alter balance, motor coordination, or locomotor activity compared with sham controls (Fig. 4b, Supplementary Fig. 21).

Devices implanted over the sciatic nerve in Advillin-ChR2 mice generate robust nocifensive responses. Wireless powering (20 Hz, 2.34 GHz RF, 3–5 dBm) of these devices produces reversible nocifensive behaviors in Advillin-ChR2 mice, but not in cre-negative littermates (Fig. 4c). These spontaneous responses are consistent with nociceptor activation. To evaluate whether optogenetic peripheral neuron activation produces behavioral aversion consistent with the perception of ongoing pain (as opposed to representing reflex activation), we place mice in a modified Y-maze apparatus where one arm is exposed to a curtained RF (LED-ON) and one arm (LED-OFF) is not (Fig. 4d). Pre-testing of devices in this arena demonstrates that activation occurs only in the LED-ON arm. Advillin-ChR2 mice demonstrate significant aversion to the LED-ON arm compared to the LED-OFF arm (Fig. 4e–f), while cre-negative littermates spend a similar amount of time in the two arms. Similarly, TrpV1-ChR2 mice, which express ChR2 only in nociceptors, demonstrate significant aversion to the LED-ON arm compared to the LED-OFF arm (Fig. 4e–f).

With the epidural devices, we demonstrate optogenetic modulation of the spinal terminals of peripheral nerves using LED devices that are inserted in the epidural space (Fig. 4g). Implantation of devices into the epidural space does not cause significant damage to the spinal cord as demonstrated histologically (Supplementary Fig. 22). Epidural device implantation also produces no impairment in motor behavior, locomotion, or coordination compared to sham controls in the accelerating rotarod and OFT (Supplementary Fig. 21). Activation of these devices (20 Hz, 2.24 GHz RF, 3–5 dBm) in the epidural space of SNS-ChR2 mice generates robust and reversible nocifensive behaviors that are entirely absent in cre-negative littermates (Fig. 4h). A Y-Arm maze assay to quantify behavioral aversion using SNS-ChR2 mice with epidural implants demonstrates robust aversion to the LED-ON arm compared to littermate cre-negative mice (Fig. 4i–j).

The miniaturized, fully implantable, thin and soft optoelectronic systems we introduce here enable robust operation and large transmission range without the need for optimization around specific cages or animal body types. The platforms are thinner by a factor of 5, more stretchable by a factor of 10, softer by a factor of 10,000, and more flexible by a factor 10,000,000 than alternative technologies, thereby providing unique features in a wide variety of optogenetic applications. The low modulus of these biocompatible devices permits experiments in body regions that would be impossible to perform with other approaches and in a chronic manner, bypassing constraints associated with the hard mechanics and thick volumetric layouts of the most recently reported fully implantable designs.[10]

Author Manuscript Author Manuscript Author Manuscript Author Manuscript

Providing easy access to this technology to the broader scientific community is essential to facilitate improved studies of neuronal circuitry. Our devices can be fabricated with 10 hours of effort using standard laboratory facilities using inexpensive commercially available components and the external power transmission systems requires less than 1 hour of training, making it possible for independent labs to construct and operate their own variants. While the hand-crafted approach to device fabrication needed for other approaches[10] offers some advantage in customization, it has limited potential to take advantage of increasingly powerful manufacturing approaches and accelerating trends in size miniaturization that drive progress in conventional optoelectronics. In contrast, our fabrication process is compatible with established flexible printed circuit board technologies and manufacturing tools from the electronics industry, making it possible to construct large numbers of devices in a cost effective manner.

Extension of our approach to multiple LEDs could enable optogenetic modulation of the whole brain or other whole organs. Laminated films with high thermal conductivity could improve the efficiency of heat dissipation, and optical diffusers could yield spatially uniform illumination. These advanced forms, as well as the present designs, have potential not only for basic research, but also as clinical tools. Gene therapy that could be used to deliver optogenetic channels to human cells is already in clinical trials[16–20], and with the appropriate testing these optogenetic stimulators could be adapted for use in treating chronic intractable human diseases such as chronic pain.

Online Methods

For all mouse studies, institutionally approved protocols are followed for all aspects of this study.

Device design and fabrication

The harvesting unit receives signals from a transmitter, rectifies them, multiplies the voltages (3x) and routes the resulting direct-current output to the LEDs. The harvesting unit is an impedance matching circuit consisting of a ceramic chip capacitor (1 pF; 0.20 mm width, 0.4 mm length, 0.22 mm thickness; bonded by solder paste) and an inductor (2.7 nH; 0.20 mm width, 0.4 mm length, 0.22 mm thickness; bonded by solder paste) connected in series. The rectifier uses miniaturized Schottky diodes (1.7 mm width, 1.5 mm length, 0.5 mm thickness) and ceramic chip capacitors (5 pF; 0.20 mm width, 0.4 mm length, 0.22 mm thickness; bonded by solder paste). The multiplier includes three Schottky diodes identical to those in the rectifier, and boosts voltages provided by the rectifier (~0.9 V) to values sufficient to operate the LEDs (~2.7 V; 220 μm width, 270 μm length, and 50 μm thickness for spinal device; 1.6 mm length, 0.8 mm width, and 0.75 mm for peripheral devices).

Fabrication begins with a clean glass slide (75 mm long, 50 mm width, and 1 mm thickness), with a layer (200 nm thickness) of polymethyl methacrylate (PMMA, 495 PMMA A6, Microchem) and a 2 μm layer of polyimide (PI) formed by spin-casting at 3000 rpm for 60 seconds, cured at 250 °C for 2 hours. Photolithography (AZ 4620, AZ Electronic Materials) defines the necessary conducting traces after e-beam deposition of Ti/Au (3 μm thickness). A second 2 μm PI layer serves as encapsulation for making a mechanically neutral plane.

Author Manuscript Author Manuscript Author Manuscript Author Manuscript

Photolithography and reactive ion etching then define the PI/metal/PI layers into serpentine-shaped structures. The LED and circuit chips are placed onto the exposed pads (Supplementary Fig. 1) with a small amount (5~20 particles) of solder paste (SMD290SNL250T5, Chipquik). The substrate is then cured at 250 °C in a vacuum oven for 10 minutes to electrically bond the LEDs and the SMD components to the conductive traces. An encapsulating layer of PDMS, spin-cast and cured at 70 °C for 1 hour seals the device prior to its release from the substrate by dissolution of the PMMA in acetone. For the epidural device, the narrow serpentine area (~360 μm width) and LED are inserted into a Teflon tube (PTFE-28-25, SAI), with an inner diameter of 380 μm. PDMS is added to the tube. The devices is cast and cured in the tube, which is then removed to complete the fabrication. The timing and steps required for device fabrication are detailed in Supplementary Table 1.

Configuration: RF system for power transmission

The RF transmission system consists of a signal generator (N5181 MXF, Agilent), a power amplifier (1189/BBM3K5KKO, Richardson RFPD), a DC power supply (U8031A, Keysight Technologies) with a heat sink (53M7972, Fischer Elektronik), and TX antennas (PE51019-3, Pasternack Enterprises) with a splitter (RFLT4W0727GN, RFLambda). The amplifier and the fan are powered by separate DC power supplies. The outputs (channels 1 & 2) connect to the J3 input of the amplifier, with VDD into Pins #6, 7 and GND into Pins #8, 9 and to the fan, respectively. The output of the signal generator connects to the input of the amplifier, which is connected to the splitter to output to all of the TX antennas.

Animals and Genetic Strategy

Adult mice (8–12 weeks of age) are utilized for this study. Mice are housed in the animal facilities of the Washington University School of Medicine on a 12 hour light/dark cycle, with access *ad libitum* to food and water. Institutionally approved protocols are followed for all aspects of this study.

Three Cre-driver lines are used for this study including heterozygous SNS-Cre mice from Rohini Kuner[21], heterozygous TrpV1-Cre mice from Mark Hoon[22], and heterozygous Advillin-Cre mice provided by Fan Wang.[14] Mice from each of these three lines are crossed to homozygous Ai32 mice from Jackson Laboratory. As previously described, Ai32 mice harbor ChR2 (H134R)-eYFP in the Gt(ROSA)26Sor locus.[23] To generate mice with conditional expression of ChR2 in specific populations of sensory neurons, mice with ChR2 in the Rosa locus (Ai32 mice) are crossed to mice expressing cre from various sensory neuron-specific driver gene loci (Advillin, TrpV1, or SNS). For the purposes of this study, the three lines generated are referred to as Advillin-ChR2, TrpV1-ChR2, and SNS-ChR2, respectively.

Surgical Procedure: Sciatic Device Implantation

The surgical procedure was modified from the Chronic Constriction Injury procedure.[24] Mice are anesthetized with isoflurane and their eyes are covered with Altalube ointment (Altaire Pharmaceuticals, Riverhead, NY) to prevent corneal drying. A small skin incision is made over the greater trochanter of the femur on the left flank of the animals. The fascia

Author Manuscript Author Manuscript Author Manuscript Author Manuscript

connecting the biceps femoris and the gluteus maximus is blunt dissected apart to open a plane between the muscles, in which the sciatic nerve is clearly accessible. The fascia connecting the underlying muscle in the area directly rostral to the incision is blunt dissected apart using needle driver forceps. The body of the device is inserted under the skin into the subcutaneous pocket generated by the blunt dissection. The gluteus maximus is pulled caudally to expose the sciatic nerve, and the tip of the device containing the LED is folded under the gluteus and placed over the nerve. The gluteus maximus is pulled over the device and sutured into place with a resorbable Ethicon 6-0 vicryl suture (Cornelia, GA) to restore the original muscle architecture, and to secure the device between the muscles and above the nerve. The left flank incision is sutured closed using Ethicon 6-0 nylon monofilament suture and the mouse is allowed to recover from anesthesia in a warmed chamber.

Surgical Procedure: Epidural Device Implantation

Under isofluorane anesthesia on an isothermal heating pad, a 2 cm midline incision is made on the back, exposing the thoracolumbar vertebral transition. The paraspinal muscles are separated, exposing the T13 spinous process and lamina. A partial laminectomy is made at the rostral end of this landmark level, allowing insertion of the epidural stimulator with the LEDs centered over the dorsal horn of the L4-L6 spinal cord segment.[25] The distal end of the epidural stimulator and proximal stretchable antenna are secured with 6-0 suture. The skin is closed utilizing interrupted sutures and mice are allowed to recover on an isothermal pad with access to food and water *ad libitum*.

Surgical Procedure: Spinal Nerve Ligation (SNL)

Mice are deeply anesthetized with vaporized isofluorane, and the paraspinal muscles are bluntly dissected to expose the L5 transverse process. The L5 process is removed, the L4 spinal nerve is tightly ligated with silk suture (6-0, Ethicon; Cornelia, GA) and the nerve is transected distal to the ligation. The skin is closed with staples and the animal is allowed to recover on an isothermal heating pad.

Surgical Procedure: Chronic Constriction Injury (CCI)

The procedure is performed as described previously.[24] In brief, mice are deeply anesthetized with vaporized isofluorane and a small incision is made over the left flank. The fascial layer between the biceps femoris and gluteus maximus is bluntly dissected to expose the sciatic nerve. Two loose chromic gut sutures are tied around the nerve, which is then reseated and the muscular architecture is re-approximated on top of it. The skin is closed with interrupted sutures, and the animal is allowed to recover on an isothermal heating pad.

Direct laser activation of the sciatic nerve in an open preparation

Mice are anesthetized with 2% isoflurane. A small skin incision is made over the greater trochanter of the femur on the left flank of the animals. The fascia connecting the biceps femoris and the gluteus maximus is blunt dissected apart to open a plane between the muscles, in which the sciatic nerve is clearly accessible. A small cutaneous incision over the lateral leg of the mouse is made, and two silver electrodes are implanted in the exposed quadriceps muscles to amplify and record electrical activity representing muscle response.

Author Manuscript Author Manuscript Author Manuscript Author Manuscript

After completion of the surgical preparation, the isoflurane anesthesia is gradually reduced over 2 hrs to ~0.875 % until a flexion reflex response (evoked by pinching the paw) is present but spontaneous escape behavior and righting reflex are still absent. The animals are not restrained in any fashion. Body temperature is maintained using an overhead radiant light and monitored throughout the experiment. These conditions are optimized to establish a stable depth of anesthesia and consistent baseline sciatic muscular activity. A laser stimulus delivered through a fiber optic cable is then used to stimulate the sciatic nerve while the EMG response is recorded in real-time using a Grass CP511 preamplifier connected to a PC via a WinDaq DI-720 module. The data are exported for analysis to Igor Pro 6.05 software (Wavemetrics, Portland, OR). Using a custom script, the EMG signals are subtracted from the baseline, rectified and integrated to quantify the area under the curve. The area under the curve for the motor response is presented in arbitrary units. The investigator quantifying the motor response is blinded to testing condition.

Behavioral Analyses

For behavioral studies, a priori power analyses were performed to estimate necessary sample sizes. However, study results demonstrated effect magnitudes larger than anticipated, and as such, increased animal numbers could not be justified. For all behavioral analyses, the experimenters were blind to genotype and treatment (implant vs. sham). Animals from each genotype were randomly selected for implant vs. sham.

Behavior: Spontaneous Behavior

Each mouse is placed in an individual plexiglass behavioral chamber. Mice are allowed to acclimate for at least 30 minutes before testing in the presence of white noise generators to reduce the influence of external noise pollution on testing. To measure spontaneous behaviors, the wireless LED devices are activated using the RF signal generator antenna at 3–5 dBm and 2.0–2.5 GHz. Behavior is recorded through an HD video camera (Sony) for one minute. Nocifensive behaviors (defined as licking hindpaws, vocalizations, or jumping) are quantified post-hoc from the video recordings while blinded to genotype.

Behavior: Y-maze

Place aversion is tested in two arms of a Y-maze constructed of plexiglass with a layer of corn cob bedding. Each arm of the maze is 10 cm wide × 100 cm long and is marked with either vertical or horizontal black stripes with a neutral area between the arms. To generate the RF signal, one antenna is located below an arm of the maze allowing for the control of LED devices through the maze floor and a second antenna is positioned on the side of the same arm to ensure complete local field coverage. To begin the experimental protocol, a mouse is placed in the neutral area of the maze and is continuously monitored and recorded through a video connection for 20 minutes. During this time an experimenter blinded to the genotype manually controls the RF signal by watching the monitoring system. Upon entry of the mouse into the “ON” chamber, activation of the LED device through the RF antenna is initiated; likewise, upon departure from the “ON” chamber RF activation is terminated. Video data are collected and time-in-chamber is analyzed using Ethovision software (Noldus, Leesburg, VA.).

Author Manuscript Author Manuscript Author Manuscript Author Manuscript

Behavior: Rotarod

The method for this technique has been described previously.[38, 39] Briefly, an accelerating Rotarod (Ugo Basile) is utilized to study motor coordination and balance after implantation of the epidural and sciatic stimulators. Five consecutive acceleration trials are performed with 5 minute breaks separating each acceleration trial.

Behavior: Open Field

As described previously, locomotion is measured in a Versamax Animal Activity Monitoring System (AccuScan Instruments) Open Field Arena.[26, 27] Mice are initially habituated to the climate-controlled test room for 1 hour before testing. Locomotor activity is assessed by recording beam breaks in this 42 (length) × 42 (width) × 30 (height) cm chamber for 1 hour. The total distance traveled during this time, time spent moving, and the number of horizontal beam breaks is calculated for the entire chamber.

DRG Culture

Lumbar DRG are dissected from 6–8 week old Advillin-ChR2, TrpV1-ChR2 or SNS-ChR2 mice in HBSS + 10 mM HEPES on ice and digested in 45U papain (Worthington Biochemical) in HBSS+H for 20 minutes at 37 °C. The tissue is washed with HBSS+H and then further digested in collagenase (1.5 mg/mL; Sigma) for an additional 20 minutes at 37 °C. After washing, cells are dissociated in Neurobasal A media (Gibco) containing 5% FBS (Life Technologies), 1× B27 supplement (Gibco), 2 mM GlutaMAX (Life Technologies) and 100 U/mL penicillin/streptomycin (Life Technologies). The tissue suspension is then filtered using a 40 μm nylon cell strainer, and centrifuged at 1000 × g for 3 minutes, resuspended, triturated, and then centrifuged 1000 × g. Neurons are resuspended in DRG media and plated onto coverslips coated with collagen and poly-D-lysine (Sigma). Cells are cultured for 3–4 days before electrophysiology experiments.

Electrophysiology

Whole-cell patch clamp recordings are made from cultured DRG neurons using pipettes with resistance values ranging from 2–3 megaohms, filled with (in mM) 120 potassium gluconate, 5 NaCl, 2 $MgCl_2$, 0.1 $CaCl_2$, 10 HEPES, 1.1 EGTA, 4 Na_2ATP, 0.4 Na_2GTP, 15 sodium phosphocreatine; pH adjusted to 7.3 using KOH, osmolarity 291 mOsm. The extracellular solution consists of (in mM): 145 $NaCl_2$, 3 KCl, 2 $CaCl_2$, 1.2 $MgCl_2$, 10 HEPES, 7 glucose; pH adjusted to 7.3 with NaOH. Recordings and light stimulation are performed using Patchmaster software (HEKA Instruments, Bellmore, NY) controlling an EPC10 amplifier (HEKA Instruments). Neurons are voltage clamped at −60 mV and held at −60 mV for current clamp recording. Optical stimulation is delivered with collimated light through the microscope objective, using a custom set-up with a blue LED (M470L2; Thorlabs) coupled to the back fluorescent port of an Olympus BX- 51 microscope. Light intensity at the focal plane (10 mW/mm^2) is calculated using a photodiode (S120C, Thorlabs) and power meter (PM100D, Thorlabs).

Author Manuscript Author Manuscript Author Manuscript Author Manuscript

Immunohistochemistry

Mice are deeply anesthetized with a ketamine, xylazine, and acepromazine cocktail, then transcardially perfused with cold 4 % paraformaldehyde in PBS. Lumbar DRG, spinal cord, and sciatic nerves are dissected and placed in 30 % sucrose in PBS for overnight cryoprotection, then frozen in OCT. Frozen tissue is then sectioned in a −20 °C cryostat (Leica) at either 30 μm (spinal cord and cross section sciatic nerve), 18 μm (DRG), or 6 μm (longitudinal sciatic nerve) directly onto frosted glass slides. IHC is conducted as described previously.[28] Goat anti-CGRP (1:400, AbD Serotec Cat# 1720-9007), rabbit anti-GFP (1:1000, Life Technologies Cat# A11122), mouse anti-NF200 (1:400, Millipore Cat# MAB5266), mouse anti-GFAP (1:500, Cell Signaling Technologies), rabbit anti-Iba1 (1:300, Wako Biochemicals cat# 019-19741), goat anti-choline acetyltransferase (1:100, EMD Millipore cat# AB144P) and mouse anti-βIII-tubulin (1:1000, Covance Research Products Inc Cat# PRB-435P-100) are utilized while IB4+ labeling is performed using an Alexa Fluor 568-conjugated IB4 (1:400, Life Technologies Cat #I21412). Research Resource IDs are provided below to assist the reader. Fluorescent-conjugated secondary antibodies (Life Technologies) are used to visualize primary immunostaining: donkey anti-goat AF647 (1:500), donkey anti-rabbit AF488 (1:500), and goat anti-mouse AF647 (1:500). Slides are sealed overnight with Prolong Gold Antifade Mountant with DAPI (Life Technologies). Images from sealed slides are obtained using a Leica SPE confocal microscope, with gain and exposure time constant throughout image groups.

Antibody	Dilution	Company	Catalog ID	Research Resource ID
Goat anti-CGRP	1:400	AbD Serotec	1720-9007	AB_2290729
Rabbit anti-GFP	1:1000	Life Technologies	A11122	AB_22156
Rabbit Anti-Iba1	1:300	Wako Chemicals	019-19741	AB-839504
Mouse anti-NF200	1:400	Sigma Aldrich	N0142	AB_2149763
Mouse anti-βIII-tubulin	1:1000	EMD Millipore	05-166	AB_291637
Goat anti-ChAT	1:100	EMD Millipore	AB144P	AB_11214092
Guinea Pig anti-GFAP	1:500	Synaptic Systems	173-004	AB_10641162
Mouse anti-GFAP	1:500	Cell Signaling Technologies	3670	AB_561049

Supplementary Material

Refer to Web version on PubMed Central for supplementary material.

Acknowledgments

This work was supported by an NIH Director's Transformative Research Award (NS081707) to R.W.G., J.A.R. and M.R.B. D.S.B. was supported by an NIH Ruth L. Kirschstein F31 Predoctoral Fellowship (1F31NS078852). C.D.M. was supported by a Howard Hughes Medical Institute (HHMI) Medical Research Fellowship. B.A.C. was supported by a W.M. Keck Fellowship in Molecular Medicine and TR32 GM108539. S.D. was supported by NS076324. Illustrations created by Janet Sinn-Hanlon and Payton Focken, University of Illinois. We would also like to think Dr. Bob Schmidt for his provided expertise in neuropathological examination of tissue.

Author Manuscript Author Manuscript Author Manuscript Author Manuscript

References

1. Iyer SM, et al. Virally mediated optogenetic excitation and inhibition of pain in freely moving nontransgenic mice. Nature biotechnology. 2014
2. Towne C, Montgomery KL, Iyer SM, Deisseroth K, Delp SL. Optogenetic control of targeted peripheral axons in freely moving animals. PloS one. 2013; 8:e72691. [PubMed: 23991144]
3. Daou I, et al. Remote optogenetic activation and sensitization of pain pathways in freely moving mice. The Journal of neuroscience : the official journal of the Society for Neuroscience. 2013; 33:18631–18640. [PubMed: 24259584]
4. Kozai TD, et al. Ultrasmall implantable composite microelectrodes with bioactive surfaces for chronic neural interfaces. Nature materials. 2012; 11:1065–1073. [PubMed: 23142839]
5. Sparta DR, et al. Construction of implantable optical fibers for long-term optogenetic manipulation of neural circuits. Nature protocols. 2012; 7:12–23. [PubMed: 22157972]
6. Jang KI, et al. Rugged and breathable forms of stretchable electronics with adherent composite substrates for transcutaneous monitoring. Nature communications. 2014; 5:4779.
7. Kim DH, et al. Epidermal electronics. Science. 2011; 333:838–843. [PubMed: 21836009]
8. Kim, T-i, et al. Injectable, cellular-scale optoelectronics with applications for wireless optogenetics. Science. 2013; 340:211–216. [PubMed: 23580530]
9. Xu S, et al. Soft microfluidic assemblies of sensors, circuits, and radios for the skin. Science. 2014; 344:70–74. [PubMed: 24700852]
10. Montgomery KL, et al. Wirelessly powered, fully internal optogenetics for brain, spinal and peripheral circuits in mice. Nat Methods. 2015; 12:969–974. [PubMed: 26280330]
11. Folcher M, et al. Mind-controlled transgene expression by a wireless-powered optogenetic designer cell implant. Nature communications. 2014; 5
12. Harrington, RF. Time-Harmonic Electromagnetic Fields. Wiley-IEEE Press; 2001.
13. Engineers, I.f.E.a.E., Vol. C95.1-2005 (2005).
14. da Silva S, et al. Proper formation of whisker barrelettes requires periphery-derived Smad4-dependent TGF-beta signaling. Proceedings of the National Academy of Sciences of the United States of America. 2011; 108:3395–3400. [PubMed: 21300867]
15. Hasegawa H, Abbott S, Han BX, Qi Y, Wang F. Analyzing somatosensory axon projections with the sensory neuron-specific Advillin gene. The Journal of neuroscience : the official journal of the Society for Neuroscience. 2007; 27:14404–14414. [PubMed: 18160648]
16. Fink DJ, et al. Gene therapy for pain: results of a phase I clinical trial. Annals of neurology. 2011; 70:207–212. [PubMed: 21796661]
17. Fink DJ, Wolfe D. Gene Therapy for Pain: A Perspective. Pain management. 2011; 1:379–381. [PubMed: 22461859]
18. Miyazato M, et al. Suppression of detrusor-sphincter dyssynergia by herpes simplex virus vector mediated gene delivery of glutamic acid decarboxylase in spinal cord injured rats. J Urol. 2010; 184:1204–1210. [PubMed: 20663524]
19. Yokoyama H, et al. Gene therapy for bladder overactivity and nociception with herpes simplex virus vectors expressing preproenkephalin. Human gene therapy. 2009; 20:63–71. [PubMed: 20377371]
20. Pleticha J, et al. Preclinical toxicity evaluation of AAV for pain: evidence from human AAV studies and from the pharmacology of analgesic drugs. Mol Pain. 2014; 10:54. [PubMed: 25183392]
21. Agarwal N, Offermanns S, Kuner R. Conditional gene deletion in primary nociceptive neurons of trigeminal ganglia and dorsal root ganglia. Genesis (New York, NY : 2000). 2004; 38:122–129.
22. Mishra SK, Tisel SM, Orestes P, Bhangoo SK, Hoon MA. TRPV1-lineage neurons are required for thermal sensation. The EMBO journal. 2011; 30:582–593. [PubMed: 21139565]
23. Madisen L, et al. A toolbox of Cre-dependent optogenetic transgenic mice for light-induced activation and silencing. Nature neuroscience. 2012; 15:793–802. [PubMed: 22446880]
24. Bennett GJ, Xie YK. A peripheral mononeuropathy in rat that produces disorders of pain sensation like those seen in man. Pain. 1988; 33:87–107. [PubMed: 2837713]

Author Manuscript Author Manuscript Author Manuscript Author Manuscript

25. Harrison M, et al. Vertebral landmarks for the identification of spinal cord segments in the mouse. NeuroImage. 2013; 68:22–29. [PubMed: 23246856]

26. Golden JP, et al. Dopamine-dependent compensation maintains motor behavior in mice with developmental ablation of dopaminergic neurons. The Journal of neuroscience : the official journal of the Society for Neuroscience. 2013; 33:17095–17107. [PubMed: 24155314]

27. Montana MC, et al. The metabotropic glutamate receptor subtype 5 antagonist fenobam is analgesic and has improved in vivo selectivity compared with the prototypical antagonist 2-methyl-6-(phenylethynyl)-pyridine. The Journal of pharmacology and experimental therapeutics. 2009; 330:834–843. [PubMed: 19515968]

28. Golden JP, et al. RET signaling is required for survival and normal function of nonpeptidergic nociceptors. The Journal of neuroscience : the official journal of the Society for Neuroscience. 2010; 30:3983–3994. [PubMed: 20237269]

Author Manuscript Author Manuscript Author Manuscript Author Manuscript

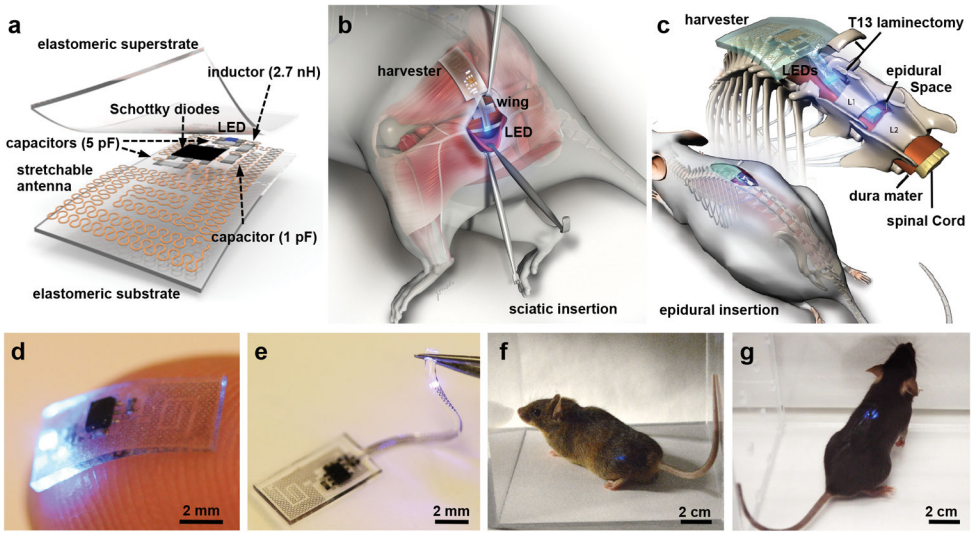

Fig. 1.

Miniaturized, fully implantable, soft optoelectronic systems for wireless optogenetics. (a) Exploded view schematic illustration of the energy harvester component of the system, with an integrated LED to illustrate operation. (b) and (c) Illustration of the anatomy and location of the peripheral and epidural devices relative to the sciatic nerve and spinal cord, respectively. (d) Picture of an active device resting on the tip of the index finger. The device is 0.7 mm thick, 3.8 mm wide, and 6 mm long; its weight is 16 mg. (e) Picture of the epidural device, highlighting the soft, stretchable connection to an LED. The diameter of the epidural implant component is 380 μm, with cross sectional dimensions comparable to the epidural space. (f) and (g) Images of mice with wireless devices implanted near the sciatic nerve and the spinal cord, respectively.

Author Manuscript Author Manuscript Author Manuscript Author Manuscript

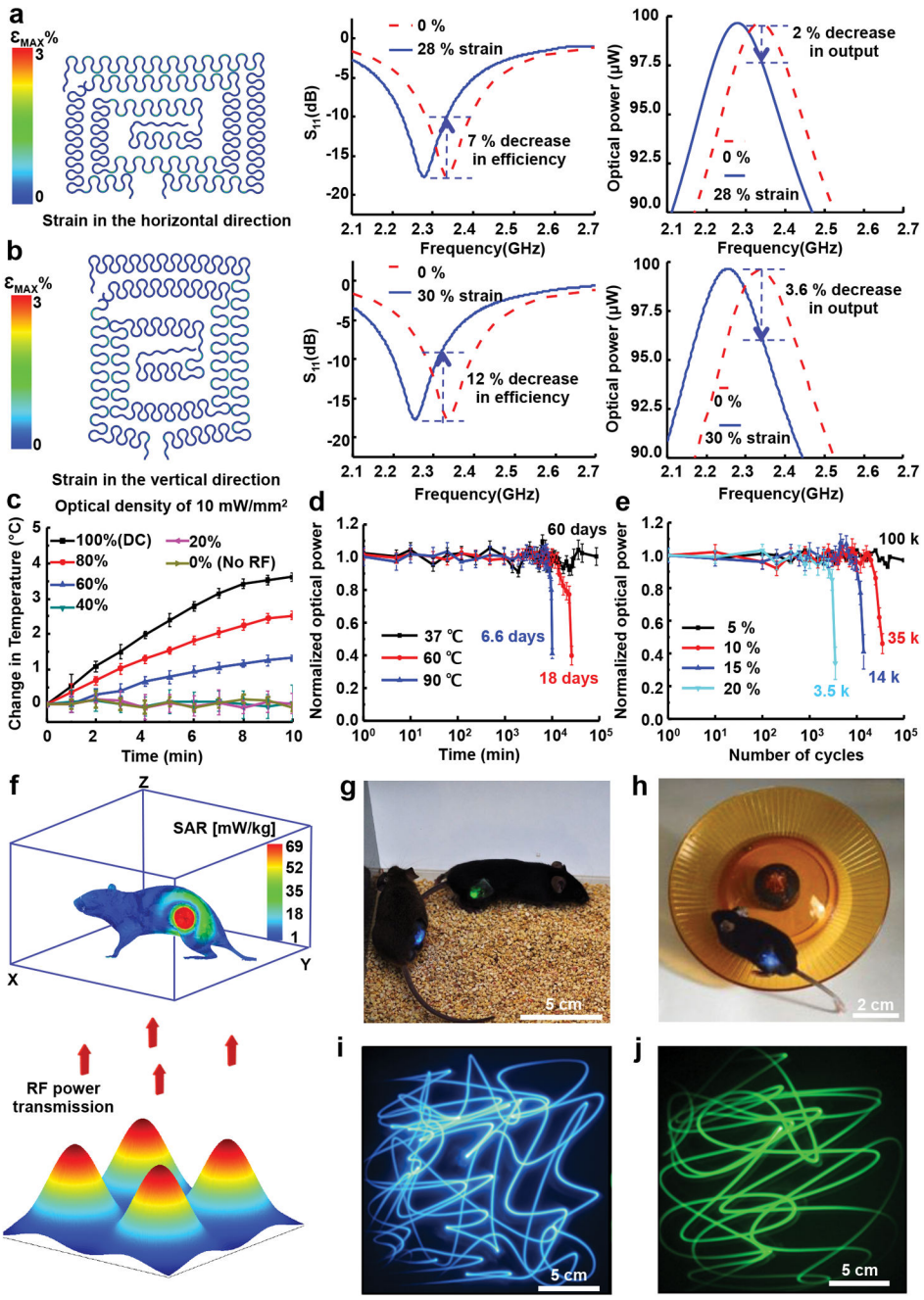

Fig. 2.

Electrical and mechanical characteristics of the stretchable optoelectronics systems. (a) and (b) Strain distributions in the stretchable antenna (left), its scattering coefficient S_{11} (middle), and corresponding optical output power (right) for strain applied in the horizontal (28 %) and vertical directions (30 %) (blue solid), respectively, and for the undeformed (0 %) configuration (red dashed). (c) *In vivo* monitoring of the temperature of a mouse at the location of an implanted device using infrared imaging, during device operation. (d) Measurements of optical output power from devices operating in saline of immersion at

Author Manuscript Author Manuscript Author Manuscript Author Manuscript

temperatures of 37 °C, 60 °C and 90 °C as a function of time. (e) Measurements of optical output power from devices subjected to cyclical application of strain with magnitudes between 5 % and 20 %. (f) Schematic illustration of the TX system and an experimental assay with computed SAR distributions on a mouse mesh body. Multiple antennas lie in the XY plane, placed below the assay. (g) Simultaneous operation of devices implanted into multiple animals in the same cage (30 × 30 cm). (h) Image of a mouse while running on a wheel with a device interfaced to the sciatic nerve. (i) and (j) Long-exposure pictures of continuous activation of LED devices manually moved through the enclosure.

Author Manuscript Author Manuscript Author Manuscript Author Manuscript

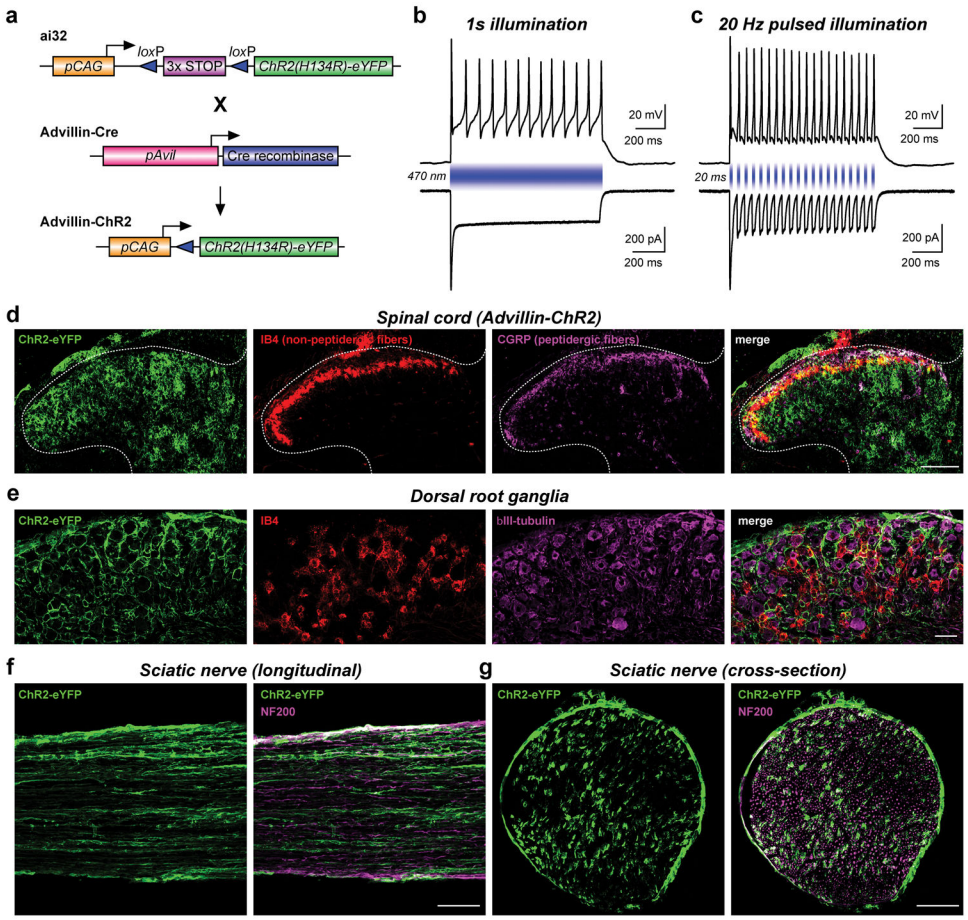

Fig. 3.

Electrophysiological and anatomical characterization of ChR2 expression in Advillin-ChR2 mice. (a) Schematic of the Ai32 locus and Advillin-Cre mouse locus where stop codons are inserted in all three reading frames and flanked by loxP sites upstream of the coding region for ChR2. The Advillin-Cre mouse locus shows Cre-recombinase driven by the sensory neuron specific *Avil* promoter. Cre recombinase expression results in recombination between loxP sites and excision of the stop codons, leading to expression of ChR2. Electrophysiological recordings from DRG neurons cultured from Advillin-ChR2 mice. For all traces, 470 nm illumination is delivered at 10 mW/mm^2. (b) 1 second-long illumination induces inward currents (lower trace) in voltage clamp recordings, and in some cells produces sustained firing in current clamp recordings (upper trace). (c) Pulsed illumination at 20 Hz induces action potential firing with high fidelity (upper trace) resulting from the inward currents that are generated in voltage clamp (lower trace). Note that the first pulse produces larger amplitude inward currents relative to the 2nd and all subsequent light pulses, consistent with the rapid desensitization to a steady-state current seen with prolonged illumination (b, lower). (d) Immunohistochemical analysis of tissue from adult Advillin-ChR2 mice demonstrates that ChR2 is expressed along the peripheral neuraxis, including termination in lamina IIo and lamina IIi of the spinal cord dorsal horn as evidenced by overlap with CGRP (purple) and IB4 (red), respectively. (e) Staining of DRG demonstrates

Author Manuscript Author Manuscript Author Manuscript Author Manuscript

significant overlap of ChR2 expression with the neuronal marker βIII tubulin (purple) and IB4 (red) within the soma. Longitudinal (f) and cross sections (g) of sciatic nerve demonstrate robust staining along the plasma membrane of the axons of both myelinated (marked with NF200, purple) and unmyelinated neurons. We also note some expression of ChR2 in the circumferential non-excitable epineurial tissue. See Supplementary Fig. 13–14 for comparison to the ChR2 expression pattern seen in TrpV1-ChR2 and SNS-ChR2 mice which, as expected, are more restricted than in these Advillin-ChR2 mice. Scale bars = 100 μm for panels d, f, g, and 50 μm for panel e.

Author Manuscript Author Manuscript Author Manuscript Author Manuscript

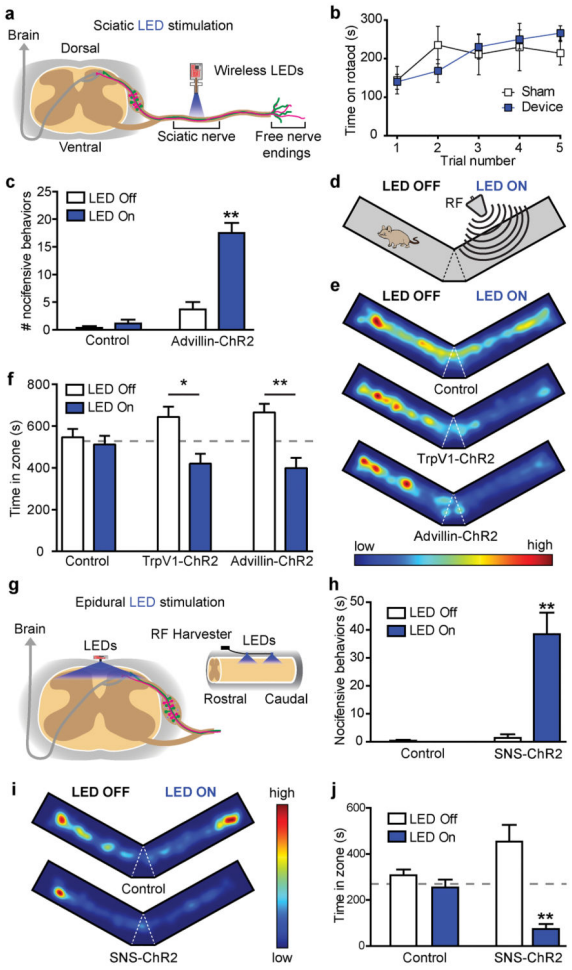

Fig. 4.

Wireless activation of ChR2 expressed in nociceptive pathways results in spontaneous pain behaviors and place aversion. (a) Representation of nociceptive pathways and illumination of nociceptive fibers with a sciatic LED stimulator. (b) Implantation of the sciatic LED stimulator has no effect on motor behavior vs. sham animals in the rotarod test ($p = 0.894$, $n = 5$ sham, $n = 8$ device). (c) Wireless activation of the sciatic LED stimulator causes increased nocifensive behaviors (flinching, hind paw licking, jumping) in Advillin-ChR2 mice but not in controls (17.5 vs. 1.2 flinches, $p < 0.0001$ vs. without illumination $n = 3$ per group). No other statistical comparisons reach significance. (d) Mice are placed in a modified Y-maze and one arm is targeted with the RF antenna to operate the LED device (LED ON) while the other is not (LED OFF). Time spent in the center area (dashed lines) is not scored (e) Heat maps from individual mice representing the time spent in each zone. Red indicates a higher amount of time, whereas blue areas indicate regions that animals occupied for less time. In animals implanted with the sciatic LED device, aversion to the LED-ON zone is observed in TrpV1-ChR2 and Advillin-ChR2 mice, but not in controls. (f) Quantification of time spent in each zone of the Y-maze. TrpV1-ChR2 (420.5 vs. 644.5 seconds; $p = 0.011$, $n = 5$) and Advillin-ChR2 (491.2 vs. 656 seconds; $p = 0.001$, $n = 8$) mice display aversion to the LED-ON zone vs. the LED-OFF zone. No difference is observed in

Author Manuscript Author Manuscript Author Manuscript Author Manuscript

control mice (547.0 vs. 512.1 seconds; p = 0.551, n = 10). (g) Representation of ascending nociceptive pathways and illumination of primary afferent terminals innervating the spinal cord with a wireless epidural implant. (h) Wireless activation of the epidural LED implant increased nocifensive behaviors in SNS-ChR2 mice (64.2 % vs. 0 % of time; p < 0.001, n = 3). (i) Heat maps representing the time spent in each zone of the Y-maze. Red indicates areas where the animals spend a higher proportion of their time. Aversion to the LED-ON zone is observed in SNS-ChR2 mice but not in controls. (j) Quantification of the time spent in each zone of the Y-maze. SNS-ChR2 mice display aversion to the LED-ON zone (73 vs. 251 seconds; p = 0.006, n = 3). No difference is observed in control mice (n = 3). Group data are presented as mean ± s.e.m. Statistical comparisons were made using two-tailed *t*-tests, except for panel B, which was a two-way ANOVA. * p < 0.05, ** p < 0.01.